

Emission modelling of hydrodynamic AGN jet simulations

Izak P. van der Westhuizen, Brian van Soelen and Petrus J. Meintjes

Department of Physics, University of the Free State,
PO Box 339, Bloemfontein 9300, South Africa,
email: vanderwesthuizenip@ufs.ac.za

Abstract. Radio-loud Active Galactic Nuclei (AGN) produce relativistic jets that can be modelled with relativistic hydrodynamic (RHD) simulations. In this study we present two such simulations of jets, used to investigate the parameters required to reproduce structures consistent with both FR I and FR II jets. In the first simulation a Lorentz factor of 10 and supersonic flow of Mach 30 were chosen, while for the second simulation a Lorentz factor of 1.0014 with a supersonic flow of Mach 4 was used. Over similar distances scales the first case shows a well collimated beam with a strong shock at the interface between the jet and ambient medium while the second case shows a less stable beam and a larger cocoon. To determine whether the simulated physical structures are consistent with the observed FR I/II jets, the synchrotron emission has been calculated to produce radio maps at a single frequency of 1.5 GHz.

Keywords. Hydrodynamic, Active Galactic Nuclei, Relativistic jets

1. Introduction

Radio-loud AGN are associated with jet-like structures which originate from the nucleus and can cover hundreds of kiloparsec in distance. These jet structures consist of collimated outflows of plasma with relativistic velocities often on the order of $\Gamma = 10$ (Urry & Padovani 1995). These jets show a complex morphology, which is dependent of both the external environment as well as intrinsic properties such as the kinetic luminosity. In general they are divided into two classes defined as FR I and FR II type jets. FR I type radio jets show the brightest emission close to the nucleus, with the jet brightness generally decreasing with distance. FR II type radio jets show collimated beams which terminate in radio lobes. The brightest components in these jets are observed as hot spots at the termination point of the jets (Fanaroff & Riley 1974; see also Torresi 2018, these Proceedings).

With the advance in computer technology numeric hydrodynamic simulations have become a powerful tool that can be used to investigate the dynamics of these jets. This is especially useful in the search for parameters which can distinguish the two different morphological classes from one another. One of the first comprehensive studies regarding the effects of injection parameters on the structure of kiloparsec relativistic jets was conducted by Martí *et al.* (1997). Several studies since have investigated various features in AGN jets such as the effects of jet composition (Scheck *et al.* 2002) and the formation of superluminal components (Aloy *et al.* 2003). Recent studies such as Rossi *et al.* (2008) and Massaglia *et al.* (2016) investigated the necessary parameters required to form FR I type jets. Both studies suggested that the deceleration of the jet beams is required to obtain physical structures consistent with FR I jets. Massaglia *et al.* (2016) estimated that the division in the FR I/FR II dichotomy occurs at a kinetic injection luminosity of 10^{43} erg.s⁻¹.

Table 1. Jet injection parameters.

Case	Lorentz factor	Density ratio	Mach number
HL	10	10^{-5}	30
LL	1.0014	10^{-4}	4

To fully determine the class of an AGN jet one must not only compare the physical structure of the jet, but also the resulting synchrotron emission. In this paper we present an estimate for the synchrotron emission of two relativistic hydrodynamic (RHD) simulations; a high Lorentz factor injection case and a low Lorentz factor injection case. The jet injection parameters were chosen to compare both the physical structure as well as the resulting emission of the two simulations.

2. Simulation setup

Two simulations were set up for this study, one to represent a decelerated beam with a low injection rate (case LL) and another with a high injection rate (case HL). The simulations were set up and evolved with time using the PLUTO code (Mignone *et al.* 2007). For the simulations a Cartesian grid was used containing $512 \times 512 \times 1024$ cells. A nozzle, with a radius of 8 cells, was created on the lower z boundary to inject jet material into the domain. The jet radius spans 100 pc in physical units, therefore the simulation domain covers an area of $6.4 \times 6.4 \times 12.8$ kpc of the outer edge of the jet.

A spherically stratified background medium was assigned to the grid with a density gradient given by,

$$\rho(r) = \frac{\rho_{am}}{1 - \left(\frac{r}{40}\right)^2}, \quad (2.1)$$

where ρ_{am} is the ambient density at the injection point and r is the distance from the injection point in beam radii.

The injection parameters of the two models are listed in Table 1. The parameters for case LL were chosen based on those shown in Massaglia *et al.* (2016) to produce FR I type structure, while similar parameters with a high Lorentz factor were chosen for case HL. In both cases a pressure matched model was used. Both simulations were evolved using parabolic interpolation and characteristic tracing time stepping.

3. Synchrotron emission estimates

To compare the physical structures of the numerical simulations to the observed Fanaroff classes, synthetic intensity maps were created of the synchrotron emission at 1500 MHz. It was assumed that the synchrotron radiation is predominantly emitted by non-thermal electrons in a single power-law distribution given by,

$$n(\gamma) = n_0 \gamma^{-p}, \quad (3.2)$$

in which $n(\gamma)$ is the number density of non thermal electrons, γ is the Lorentz factor, $p = 2.1$ is the photon index and n_0 is a normalization factor. The non-thermal spectrum is normalized to the internal energy and number density of the fluid as was done in previous studies such as Gomez *et al.* (1995).

Based on the power-law spectrum emission and absorption coefficients were calculated for each cell in the simulation using the δ -approximation (see e.g. Böttcher 2012) and integrated along a chosen line of sight. Relativistic effects and light travel time were taken into account during integration, however, cosmological corrections were neglected.

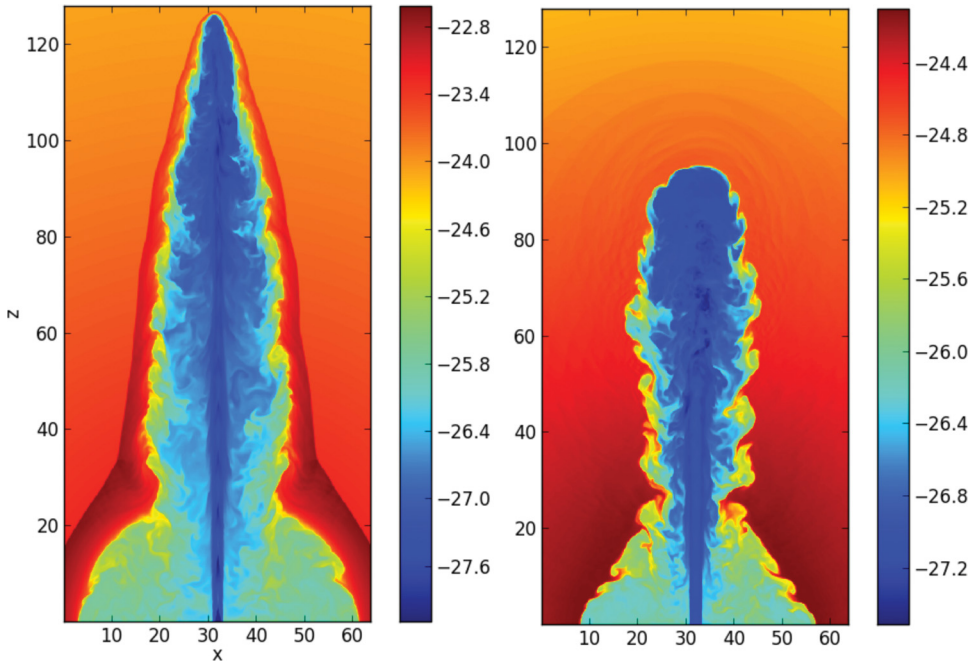


Figure 1. Density slices through the xz -plane of the simulations for Case HL (left) at a time of 9.5×10^4 yr and Case LL (right) at a time of 2.4×10^6 yr. Logarithmic scales are shown for the density plots in units of g.cm^{-3} .

4. Results

The LL simulation was evolved for a time of 2.4×10^6 years. At this stage the propagation of the jet into the ambient medium became negligible, with only the cocoon increasing in size as more matter is injected. A cross-section of the density is shown in Figure 1 and is consistent with the structure obtained by [Massaglia *et al.* \(2016\)](#). In this simulation the jet beam becomes unstable after 40 beam radii, the bulk velocity of the jet fluid is decelerated and the jet breaks down before it can reach the interface with the ambient medium.

The HL model was evolved for a simulation time of 9×10^4 years. At this stage the head of the jet exceeded the upper z boundary and the evolution could no longer be simulated. The high Lorentz factor model shows a well collimated beam which terminates in the interface between the jet and ambient medium, the working surface. This leads to the formation of a shock front at which the kinetic energy of the fluid is converted into internal energy. The cocoon of this model is narrow when compared to AGN radio lobes. It is expected that the jet will propagate over a larger distance into the ambient medium forming a more extended cocoon as more material is injected. A strong bow shock is also observed enveloping the jets structure.

Intensity maps were calculated for the two models at the same time step and are shown in Figure 2. Despite the difference in physical structure both of the simulations show intensity maps more consistent with FR II type radio jets. The LL model shows a region of uniform increased intensity at the jet head while the HL model shows the presence of a more filamentary structure with brighter emission.

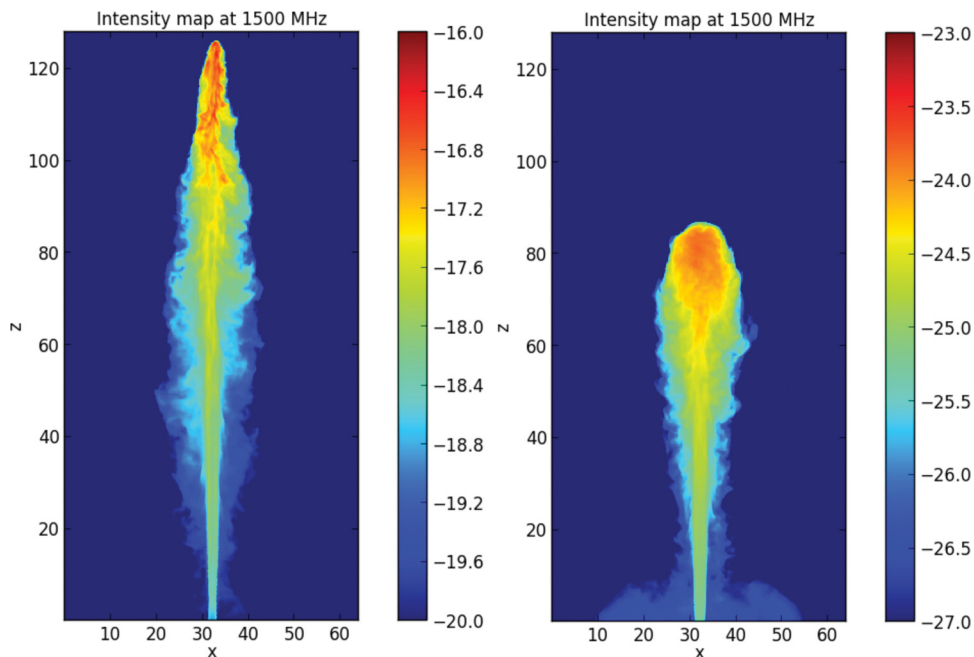


Figure 2. Intensity maps plotted for a viewing angle of 90° relative to the injection direction for Case HL (left) at a time of 9.5×10^4 yr and Case LL (right) at a time of 2.4×10^6 yr. The intensity is shown in a logarithmic scale of arbitrary units at a frequency of 1500 MHz.

5. Conclusion

In this paper two RHD simulations of AGN jets are shown. The simulations were set up to study the difference in structure between high and low Lorentz factor jets. The High Lorentz factor (HL) simulation showed physical structures which have been associated with that of FR II type jets and propagated past the domain of the simulation. In the Low Lorentz factor (LL) simulation the propagation of the jet slowed down before it reached the edge of the domain. The beam of the jet also destabilized before it reached the head of the jet. This structure is more consistent with that of FR I type jets.

Intensity maps were calculated for both simulations and showed an increase in emission with distance from the injection nozzle. This is in contrast with the physical structure which was obtained. Additional investigation is ongoing to determine the cause of this effect. The results may suggest that the effects of a decelerated beam alone is not enough to reproduce the FR I type emission structures. It is, however, possible that effects such as radiative cooling may change the observed structure over time. Improved emission modelling is being implemented in the form of Monte-Carlo methods to obtain a self-consistent spectrum that will allow us to better investigate the emission structures which form in these simulations.

References

- Aloy, M. A., Martí, J. M., Gómez, J. L., Agudo, I., Müller, E., & Ibáñez, J. M., 2003, *ApJ*, 585, 109
- Böttcher M., Harris D. E. & Krawczynski H., 2012, *Relativistic Jets from Active Galactic Nuclei*, Wiley-VCH Verlag GmbH & Co. KGaA, Weinheim, Germany, Chapter 3, pp 39-80
- Fanaroff B. L. & Riley J. M. 1974, *MNRAS*, 167, 31

- Gomez J. L., Marti J. M., Marscher A. P., Ibáñez J. M. & Marcaide J. M., 1995, *ApJ*, 449, 19–21
- Martí, J. M., Müller, E., Font, J. A., Ibáñez, J. M. & Marquina 1997, *ApJ*, 479, 151
- Massaglia S., Bodo G., Rossi P., Capetti S., & Mignone A., 2016, *A&A*, 596, 10
- Mignone A, Bodo G, Massaglia S, Matsakos T, Tesileanu O, Zanni C & Ferrari A 2007, *ApJ*, 170, 228–42
- Rossi P, Mignone A, Bodo G, Massaglia S & Ferrari A, 2008 *A&A* 488, 795–806
- Scheck, L., Aloy, M. A., Martí, J. M., Gómez, J. L., & Müller, E. 2002, *MNRAS*, 331, 615
- Torresi E., 2018, *Proc. IAU Symposium No. 342*, (S342)
- Urry, C. M. & Padovani, P. 1995, *PASP*, 107, 803